



## RESEARCH LETTER

10.1002/2015GL065003

## Key Points:

- Noble gases make excellent tracers of meltwater in Greenlandic fjords
- Resolved glacially modified water distribution illuminates ice-ocean interaction
- Different melt plume regimes are found in front of a glacier

## Supporting Information:

- Texts S1–S7, Figures S1–S4, and Tables S1 and S2

## Correspondence to:

N. Beaird,  
nbeaird@whoi.edu

## Citation:

Beaird, N., F. Straneo, and W. Jenkins (2015), Spreading of Greenland meltwaters in the ocean revealed by noble gases, *Geophys. Res. Lett.*, 42, 7705–7713, doi:10.1002/2015GL065003.

Received 18 JUN 2015

Accepted 6 SEP 2015

Accepted article online 11 SEP 2015

Published online 30 SEP 2015

## Spreading of Greenland meltwaters in the ocean revealed by noble gases

Nicholas Beaird<sup>1</sup>, Fiammetta Straneo<sup>1</sup>, and William Jenkins<sup>2</sup>

<sup>1</sup>Department of Physical Oceanography, Woods Hole Oceanographic Institution, Woods Hole, Massachusetts, USA, <sup>2</sup>Department of Marine Chemistry and Geochemistry, Woods Hole Oceanographic Institution, Woods Hole, Massachusetts, USA

**Abstract** We present the first noble gas observations in a proglacial fjord in Greenland, providing an unprecedented view of surface and submarine melt pathways into the ocean. Using Optimum Multiparameter Analysis, noble gas concentrations remove large uncertainties inherent in previous studies of meltwater in Greenland fjords. We find glacially modified waters with submarine melt concentrations up to  $0.66 \pm 0.09\%$  and runoff  $3.9 \pm 0.29\%$ . Radiogenic enrichment of Helium enables identification of ice sheet near-bed melt ( $0.48 \pm 0.08\%$ ). We identify distinct regions of meltwater export reflecting heterogeneous melt processes: a surface layer of both runoff and submarine melt and an intermediate layer composed primarily of submarine melt. Intermediate ocean waters carry the majority of heat to the fjords' glaciers, and warmer deep waters are isolated from the ice edge. The average entrainment ratio implies that ocean water masses are upwelled at a rate 30 times the combined glacial meltwater volume flux.

## 1. Introduction

The Greenland ice sheet is shrinking at an accelerating rate, contributing significantly to sea level rise [Hanna *et al.*, 2013] and increasing freshwater discharge to the North Atlantic [Bamber *et al.*, 2012]. Model skill in predicting ice sheet evolution, and thus sea level rise and ocean freshwater input, is inhibited by incomplete knowledge of coupled ice-ocean dynamics [Straneo *et al.*, 2013]. Ocean forcing likely impacts ice-sheet dynamics via marine-terminating glaciers [Holland *et al.*, 2008; Nick *et al.*, 2014]. Processes at the ice-ocean boundary also control the vertical distribution of freshwater input to the ocean, with implications for large-scale ocean circulation [Straneo *et al.*, 2011; Straneo and Heimbach, 2013].

Glacially modified water (GMW) is seawater whose temperature, salinity, and chemical characteristics have been altered by interaction with a marine-terminating glacier. These changes are caused by submarine melting and/or injection of meltwater-runoff that originates in the interior of the ice sheet. GMW contains freshwater forcing from Greenland to the ocean and also carries information on processes at the ice-ocean boundary. As such, the distribution and properties of GMW offer an integrated view of fjord circulation and ice-ocean interaction. Indeed, many studies of Greenland glacier-fjord systems use GMW characteristics either to infer circulation or reconstruct quantities such as submarine melt rates [Straneo *et al.*, 2011, 2012; Bartholomaeus *et al.*, 2013; Mortensen *et al.*, 2013; Chauché *et al.*, 2014; Inall *et al.*, 2014; Gladish *et al.*, 2015; Bendtsen *et al.*, 2015]. Tracing GMW is particularly valuable for short surveys because energetic, nontidal, currents frequently alias synoptic velocity measurements, masking glacially driven circulations [Sutherland and Straneo, 2012; Jackson *et al.*, 2014].

Because runoff and submarine melt alter seawater in characteristic ways [Jenkins, 1999], GMW is often identified by assessing apparent changes in temperature-salinity ( $\theta/S$ ) space, for example, by finding  $\theta/S$  mixing lines with slopes characteristic of submarine melt-seawater mixing. This technique, sometimes referred to as melt line or “Gade slope” analysis [e.g., Gade, 1979; Straneo *et al.*, 2011; Chauché *et al.*, 2014], is a variant of traditional water mass analysis in which several known end-member water types are defined (e.g., ocean water types, runoff, and submarine melt), and the contribution of each end-member type to a mixture (e.g., GMW) can be quantitatively evaluated under certain conditions. Formally, water mass analysis amounts to solving a set of linear mixing equations. The analysis requires that there be at least as many observed conservative tracers (e.g.,  $\theta$  and  $S$ ) as unknowns (the number of water types in the mixture). Using this analysis one can in principle identify GMW and quantify the fraction of runoff and meltwater in GMW.

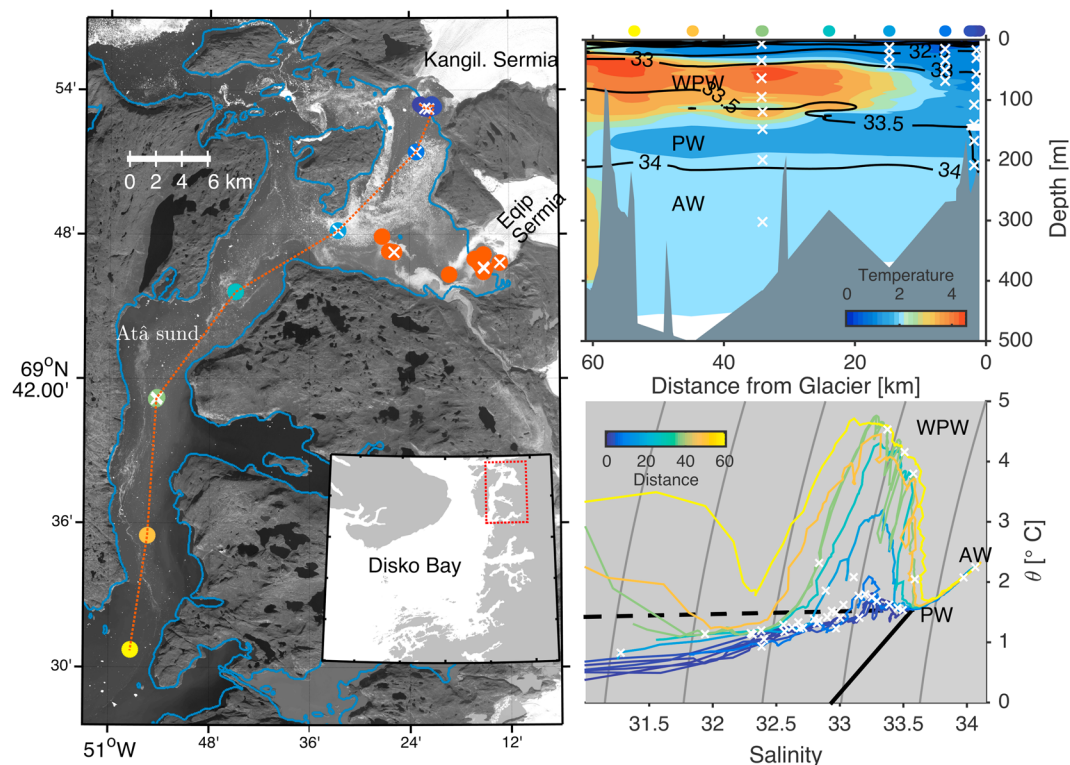


**Figure 1.** (left) Contemporaneous Landsat image showing hydrographic stations (colored dots), and noble gas measurements (crosses) in Atâ Sund, and in front of Kangilerngata Sermia and Eqip Sermia in 2014. Inset map shows the location within the Disko Bay region. (top right) Potential temperature ( $^{\circ}\text{C}$  colored contours) and salinity (black contours) section along the dotted line in the map (see bathymetry note in the supporting information). Hydrographic stations marked at top with colored dots, water samples marked by crosses. (bottom right) Corresponding profiles and samples in potential temperature-salinity space with profiles colored by distance from the Kangil in kilometers (color scale the same for the Hydrographic stations on the map and above the temperature section). Oceanic  $\theta/S$  end-members Atlantic Water (AW), Polar Water (PW), and Warm Polar Water (WPW) are shown. Mixing lines from PW to SMR (dashed) and SMW (solid) are shown.

Unfortunately, in most cases around Greenland too few tracers are observed to account for the number of water types present. Many of Greenland's proglacial fjords contain at least two (seasonally three) oceanic water types: a warm, salty Atlantic Water derivative; a cold, fresh Polar Water derivative; and seasonally a warm, fresh, Polar Water variant (e.g., Figure 1) [Straneo et al., 2012]. Submarine Meltwater (SMW), the product of ice melting directly into the ocean, adds another type [Jenkins, 1999]. Away from the ocean, freshwater is produced primarily by surface melt but also by melting within and at the base of the glacier by frictional and geothermal heating [Chu, 2014]. This Surface Melt Runoff (SMR) flows out from under the base of marine-terminating glaciers mixing with the other types. The most commonly used tracers are temperature and salinity, which, including mass conservation, provide only three constraints for five unknowns—leaving the water mass analysis underconstrained.

Much previous work that attempts to identify GMW ignores the problem by explicitly or implicitly assuming that only a single oceanic water mass is present. This assumption can lead to serious errors in interpretation of the distribution and properties of GMW. The issue is particularly acute because mixing between AW and PW very often falls along a melt line (Gade slope) in  $\theta/S$  space [e.g., Straneo et al., 2012, Figure 2].

In this paper we outline and implement a method to trace and decompose GMW sourced from Greenland's glaciers using noble gases and helium isotopes as conservative tracers. With the additional tracers, the system of mixing equations becomes overdetermined and can be solved using a minimization routine to best determine the constituent water types [Tomczak and Large, 1989]. The method builds on techniques developed to trace meltwater around Antarctica [Schlosser, 1986; Hohmann et al., 2002; Loose et al., 2009; Loose and Jenkins, 2014] but is extended to account for additional meltwater types found on the warmer Greenlandic ice sheet.

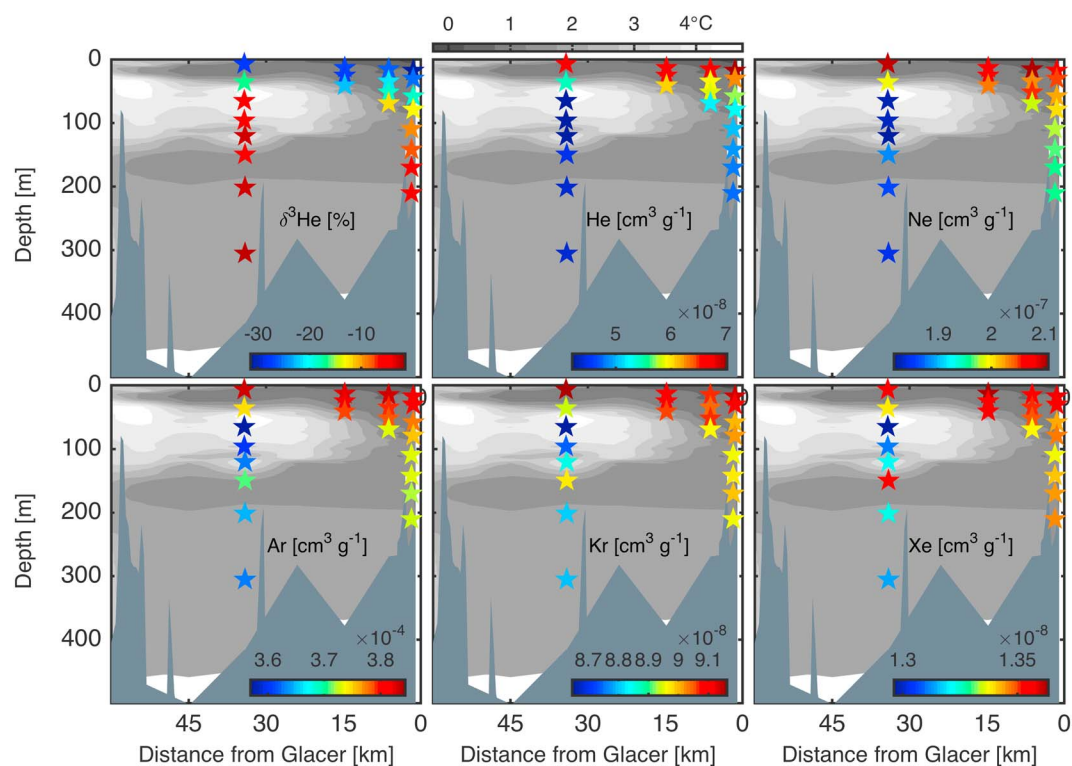


**Figure 2.** Noble gas concentrations ( $\text{cm}^3 \text{STPg}^{-1}$ ) and He isotope ratio anomaly ( $\delta^3\text{He}$  [%]), colored stars, on the section (Figure 1) up to Kangil. Temperature section from Figure 1 is shown in grayscale in the background.

The method provides a powerful tool for investigating ice-ocean interaction processes by unambiguously quantifying the composition and distribution of GMW.

We use the method to quantify water mass distribution in Atå Sund, West Greenland, and transformation driven by the two marine-terminating glaciers at the head of the fjord: Kangilerngata Sermia and Eqip Sermia (Kangil and Eqip, Figure 1), grounded in 300 m and 90 m of water, respectively [Rignot *et al.*, 2015].

## 2. Sample Collection and Analysis

Noble gas samples and hydrographic observations were collected in late August 2014 in Atå Sund, adjacent to Disko Bay (Figure 1). Potential temperature, salinity, and turbidity measurements were made using an RBR XR-620 CTD. Fifty-five water samples (Figure 2) were collected and sealed in copper tubing. Analysis was completed at Woods Hole Oceanographic Institution (WHOI)'s Isotope Geochemistry Facility using a well-established technique [Jenkins *et al.*, 2014] (also see supporting information). Duplicate samples were taken for each of the 55 water samples, and 11 pairs were analyzed, showing good agreement ( $\sim 0.15\%$  average standard deviation of duplicates).

## 3. Quantifying Glacial Melt in Seawater

In Antarctica, where annual average surface temperatures are largely below freezing, SMW is the dominant form of freshwater delivered to the ocean from the ice sheet [Foldvik *et al.*, 2004]. Air temperatures in Greenland are more temperate, producing SMR from seasonal surface melt of the ice sheet. Combined with some interior and basal melting, this runoff enters the fjord at depth [Chu, 2014]. Both SMW and SMR impart buoyancy forcing to the ocean and drive convective circulations when injected into a salt stratified fjord. But they reflect different processes of ice-ocean-atmosphere interaction, and thus, we can learn about the system by characterizing them separately.

Noble gases (He, Ne, Ar, Kr, and Xe) exhibit physical behaviors that produce very strong signals to differentiate SMW, SMR, and oceanic source water types in a mixture. Noble gases do not undergo chemical or biological reactions in the ocean and hence are conservative tracers. They are affected only by boundary processes

involving exchange with the atmosphere [Hamme and Severinghaus, 2007; Stanley et al., 2009] and ice [Hood et al., 1998; Loose and Jenkins, 2014]. Their advantage as tracers lies in part in a tenfold difference in aqueous solubility between He (least soluble) and Xe (most) and a tenfold range in the temperature dependence of that solubility [Loose and Jenkins, 2014].

The additional tracers create an overdetermined set of mixing equations and permit the use of an enhanced form of traditional water mass analysis known as Optimum Multiparameter Analysis (OMP) [Tomczak and Large, 1989]. Given more tracers than water masses, the OMP finds the mixture of end-members that minimizes the residual misfit between an observation and the linear combination of end-members (see supporting information for details). The critical step in implementing the OMP is defining the end-member tracer values and assigning relative weights to the constraint equations.

### 3.1. End-Member Water Types

Two classes of end-members are defined: far-field ambient oceanic water masses and the types of meltwater derived from glacial ice. The OMP is constructed from these definitions, which are explained below and recorded in Table S1 in the supporting information.

#### 3.1.1. Oceanic Sources

Temperature and salinity sections show three oceanic water types present at the entrance to Atâ Sund (Figure 1), such that the  $\theta/S$  profiles farthest from the glacier can be approximated by mixing lines between three points. This excludes a near-surface layer clearly modified by glacial influence. We define the ambient ocean end-member water types to be Atlantic Water (AW), Polar Water (PW), and Warm Polar Water (WPW), whose temperature and salinity end-member values are determined by inspection of  $\theta/S$ . For each end-member, noble gas and isotope values are defined from the water sample that is closest in thermohaline space to the  $\theta/S$  definition for that water type. The definitions are thus proximal end-member values for AW, PW, and WPW and will include any modification due to glacial interaction outside of Atâ Sund.

#### 3.1.2. Glacial Sources

We define two main types of glacial end-members: SMW and SMR. In addition, we identify Ancient Ice Melt (AIM)—melting of ice that has accumulated terrigenically produced He over time—which could represent additional SMW, or melting near the base of the ice sheet away from the ocean.

Latent heat associated with melting ice produces different temperatures for SMR and SMW. The latent heat required to produce SMR is exchanged at the ice sheet surface (atmosphere-ice boundary), and we assume that SMR enters the ocean with a temperature near 0°C. SMW, on the other hand, requires latent heat drawn from the ocean to undergo the phase change. This may be expressed by an effective temperature of SMW,  $\theta_{SMW}^{eff} = -87^\circ\text{C}$ , that includes the heat required to warm the ice to the freezing point, the latent heat required for the phase change, and assumes that the meltwater produced is at the freezing point (Gade [1979] and supporting information).

Because SMR is formed on the surface of the ice sheet and is isolated from the atmosphere once it drains from the surface, noble gas end-member properties for SMR are determined by assuming that it is in solubility equilibrium with the atmosphere (supporting information). Supraglacial lakes and rivers that collect SMR before it drains tend to be shallow, and we expect that the water will be in equilibrium with the atmosphere at zero salinity and a temperature near 0°C [Chu, 2014].

As layers of snow are compacted into ice in the accumulation zone of a glacier, pockets of air are sealed off, forming bubbles that leave atmospheric concentrations of gas suspended in the ice matrix. When this ice is melted under pressure, as with SMW or AIM, trapped bubbles dissolve into the meltwater mixture, creating anomalous noble gas concentration signals which can be traced even in extremely dilute quantities [Schlosser, 1986]. This process of bubble dissolution coupled with the range of aqueous solubility and atmospheric partial pressures of the noble gases makes these gases excellent tracers of SMW and AIM. SMW and AIM noble gas concentrations are determined using published values of mean air content in the ice [Martinierie et al., 1992]. Additionally, the gas content of the ice bubbles must be adjusted for gravitational separation which occurs in the firn layer [Craig et al., 1988].

Ice near the bedrock experiences enrichment of He isotopes from radiogenic sources (Craig and Scarsi [1997] and supporting information). We use the He abundance and isotope signature of this radioactive decay to identify AIM. There is some ambiguity in the origin of AIM, which could possibly be produced by submarine melting of old ice at the glacier terminus or melting of old ice near the base of the glacier by geothermal or frictional heating (see supporting information).

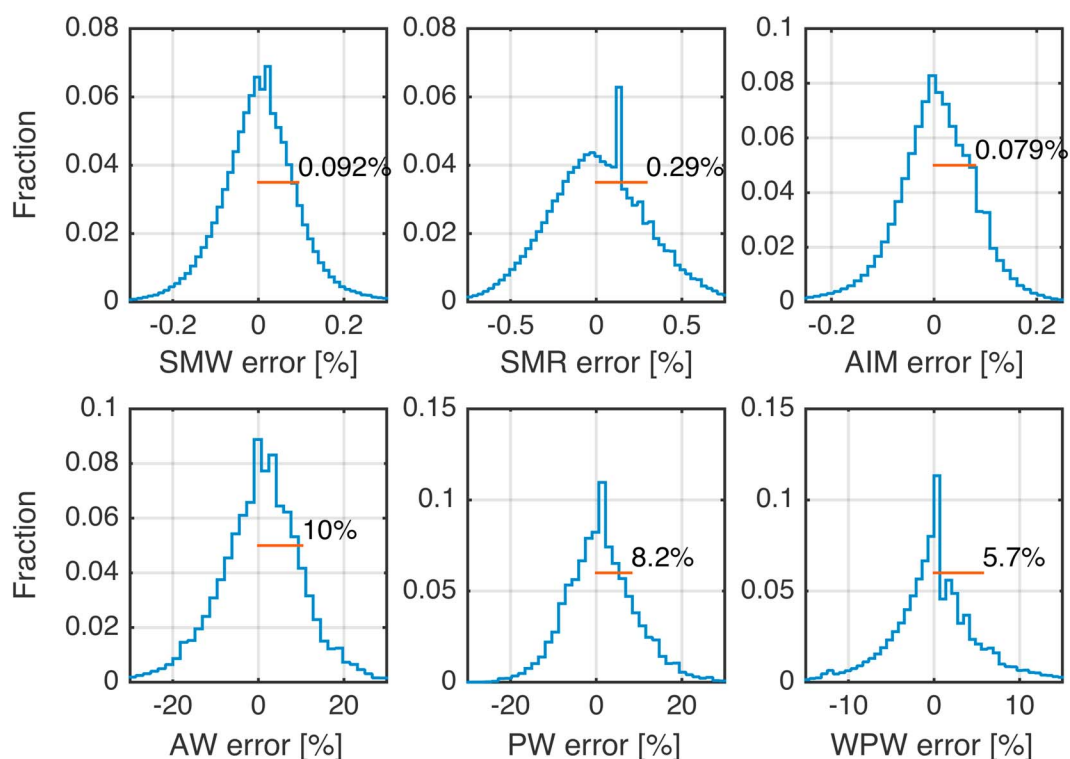


**Figure 3.** The distribution of the differences between Monte Carlo perturbed fractions and the unperturbed fractions for each end-member in the OMP. The standard deviation of the distribution is given by the red bar in each panel and taken to represent the error.

### 3.2. Uncertainty

Uncertainty in the results of the OMP is assessed by Monte Carlo simulation. Each end-member tracer value is perturbed according to a random normal distribution with a mean equal to the chosen end-member value (Table S1) and a standard deviation that reflects the uncertainty in that value (see supporting information). The OMP system is solved for 550,000 perturbed realizations of end-member properties, and the standard deviation of differences between the perturbed and unperturbed solution are taken as the model uncertainty (Figure 3). The uncertainty is much smaller for glacial components (SMW = 0.09%, SMR = 0.29%, and AIM = 0.08%) than for the oceanic end-members (AW = 10%, PW = 8.1%, and WPW = 5.7%) (Figures 3 and S4).

## 4. Results

Noble gas/OMP-derived profiles of water mass fraction illuminate the distribution and composition of GMW. Sampling was sparse away from the glaciers, but coverage in  $\theta/S$  space was more complete (Figure 1), allowing us to interpolate the OMP results in  $\theta/S$  space onto the complete CTD data set. Figure 4 shows the full OMP-derived water mass distribution along the fjord.

Far from the glaciers, and below a layer of GMW (0–60 m, where SMW, SMR, and AIM >0), the undisturbed distribution of oceanic water masses is revealed by the OMP (Figure 4): AW dominates from 175 m to the bottom, PW sits above that (125–175 m), and WPW occupies the 60–125 m range. Within 20 km of the glaciers the noble gases and OMP reveal a radical vertical redistribution of water masses induced by glacial interaction. PW concentrations are high throughout the water column, while AW and WPW concentrations are low. We find SMW, SMR, and AIM present throughout the full water column near the glacier, indicating full-depth glacial modification. SMR and AIM concentrations are maximum at the surface, while close to the glaciers SMW concentrations remain relatively high to the bottom. AIM is strongly correlated with SMR (Figure 4), suggesting that it might reflect interior melt near the glacier base carried to the sea along with SMR.

The injection of buoyant glacial freshwater drives turbulent, convective plumes, which entrain, redistribute, and modify ocean water masses to create GMW. We find that GMW in Atâ Sund is predominantly composed of entrained PW. SMW, SMR, and AIM concentrations vary between 0.1–0.66% (SMW) and 0.21–3.9% (SMR)

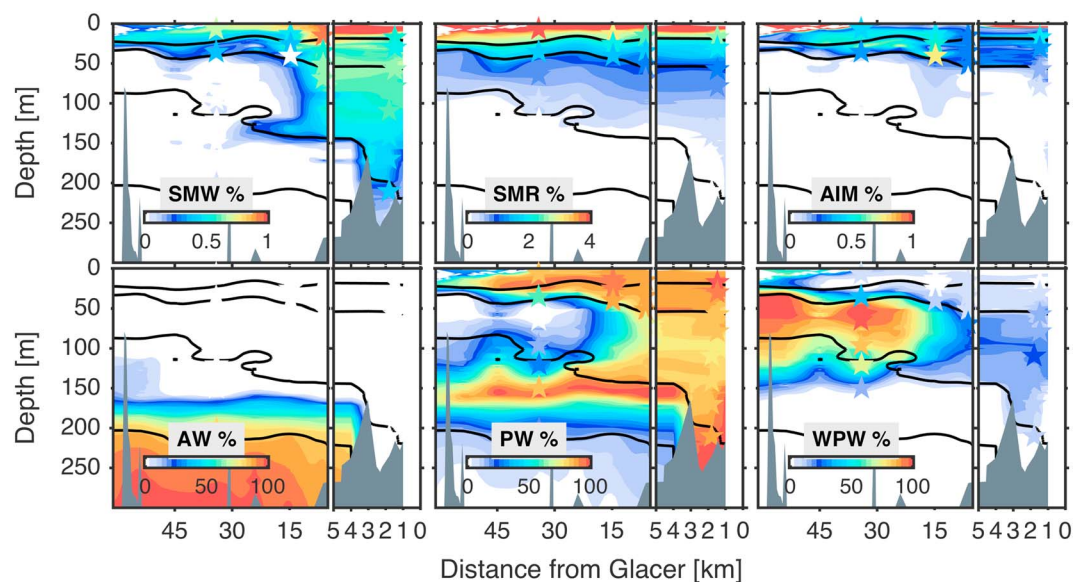


**Figure 4.** OMP-derived sections up to Kangil (Figure 1) showing water mass concentration in the upper 300 m. Colored contours are OMP solutions interpolated onto CTD  $\theta/S$  data, and colored stars show solutions at the water sample locations. Salinity contours from Figure 1 in black contours. The concentration of all end-members are zero below 300 m, except AW, which is 100%. Color bars show the range of concentration for each panel. Note expanded distance scale close to the glacier.

and 0.05–0.48% (AIM) in the GMW. Thus, glacial sources comprise just 0.6–5% of the GMW in the fjord. The majority of the GMW volume is made of entrained ambient water: approximately 80% PW, 10–15% WPW, and 0–10% AW (Figure 4).

A shallow sill ( $\sim 160$  m) sits about 2.5 km in front of Kangil's terminus, forming a small proglacial basin (Figure 4 and supporting information). The dominance of PW, and relative lack of AW found in the GMW, suggests that the PW is able to regularly flow over this sill and fill the basin where it both melts the glacier terminus and mixes with SMR injected at the glacier base. At the time of this survey, however, AW was mostly blocked from contact with the glacier, and only a small amount is present in the GMW in the proglacial basin (Figure 4). It is the PW, therefore, that primarily interacts with the glacier, carrying heat for melting and being entrained and upwelled in the GMW plume. WPW is also present in small quantities in the GMW.

Close inspection of  $\theta/S$  profiles shows isopycnal interleaving between the GMW and WPW at middepth, fed by a layer of SMW intruding along the 33.5 isohaline. This interleaving implies export of GMW at depth, primarily SMW rather than SMR, and import of WPW toward the glacier. This subsurface export of meltwater has been observed in other stratified fjords [Straneo *et al.*, 2011] but is not considered in the type of two-layer heat, mass, and salt budgets previously used to calculate melt rates in Atâ Sund [Rignot *et al.*, 2010].

## 5. Discussion

The noble gas/OMP method highlights the main aspects of the glacier-fjord system, including pathways of ocean waters to the glacier, levels of turbulent entrainment, meltwater plume characteristics, and relative rates of submarine melting and runoff. It also allows clear disambiguation of the water mass structure. With the noble gas OMP, we remove the ambiguity associated with differentiating GMW from the AW-PW mixing line, which lies close to the Gade slope and can be misinterpreted as AW-SMW mixing. With standard  $\theta/S$  analysis commonly used in Greenland, many nonunique interpretations of the water mass structure are possible. In particular, the presence of SMW at depth close to Kangil would be nearly impossible to detect. Also, the *lack* of AW at the terminus of Kangil could easily be missed (as in Rignot *et al.* [2015]).

Entrainment rates can be estimated from our observations as the ratio of ocean water mass fraction to the combined SMR, AIM, and SMW fraction in the GMW. This ratio is large, indicating that the total GMW formed near the surface by glacier-driven buoyancy forcing is many times larger than the total freshwater input at depth, and much of the GMW volume is drawn from deep water masses. In Atâ Sund, the average entrainment

ratio implies that the PW volume upwelled is approximately 30 times the combined SMR and SMW volume flux. This illustrates a major impact of glacial buoyancy forcing: entrainment in the GMW plumes redistributes oceanic water masses vertically. This is true wherever tidewater glaciers around Greenland terminate in stratified water and has implications for the vertical transport of heat and nutrients, as well as potential seasonal modulation of boundary currents.

By quantifying all end-members separately, we find that the ratio of SMW to SMR near the glacier increases with depth (from 0.12 to 2.3). This suggests multiple melt processes occurring at the ice-ocean interface. Near the surface, SMR dominates SMW, characteristic of GMW produced by convection-driven melt where SMR drives strong vertical motion, enhances melting, and equilibrates at the surface [Jenkins, 2011; Xu et al., 2013; Slater et al., 2015]. Deeper in the proglacial basin, SMW dominates over SMR, reminiscent of melt-driven convection with thermally driven melting where GMW equilibrates deeper in the water column [Wells and Worster, 2008]. The melt-driven convection regime is sensitive to changes in ocean temperature, while the convection-driven melt regime will respond to ocean temperature changes and the atmospheric forcing that produces SMR. Modeling studies often focus on the submarine melting associated with the SMR-driven plumes [Xu et al., 2013; Sciascia et al., 2013; Kimura et al., 2014; Slater et al., 2015], yet here we see significant SMW at depth that is not accompanied by high SMR concentrations.

In the near-surface GMW, where both SMW and SMR are present, we find a mean ratio of SMW to SMR of 0.26. Assuming that the collocated SMW and SMR fields are advected by the same circulation, the lower limit estimate of SMW volume flux is  $\geq 26\%$  of the SMR volume flux. Rignot et al. [2010] report ratios of SMW to SMR volume flux of 6.7% and 4.5% for Kangil and Eqip, respectively. Our observations indicate that relative melt rates are either 4 times as high in summer 2014 or assumptions used to calculate previous melt rates may be invalid. The subsurface export of SMW highlighted by the OMP violates assumptions used to calculate melt rates in Rignot et al. [2010] and could contribute to the discrepancy between our observed SMW to SMR ratio and that inferred in the previous work.

AIM to SMR ratios indicate that AIM volume could be roughly 13% of the SMR flux. The origin of this AIM is uncertain and should be thought of as some combination of the basal melt in the englacial hydrologic system, and the submarine melt of the glacier terminus where excess He from bedrock sources is present. The AIM distribution thus reflects either higher submarine melt rates or a considerable amount of melt at the interior glacier base.

## 6. Conclusions

We show that noble gases can unambiguously, and sensitively, trace meltwater components and water mass modification in a Greenlandic glacier/fjord system. The combination of the gases and the OMP resolves serious indeterminacy issues inherent in standard water mass analysis of Greenland's fjords. By better constraining the water mass analysis, the method provides a powerful new tool to investigate pathways of freshwater export toward the ocean, transport of heat toward glaciers, and ice/ocean boundary processes.

The method shows that glacial meltwater (SMR, AIM, and SMW) in Atâ Sund are exported both at the surface and depth. This implies that subsurface and surface measurements are required to monitor freshwater export from Greenland's glaciers. Deep meltwater pathways call into question the validity of two-layer models used to calculate melt rates in fjords. Export of GMW at depth also indicates that some GMW equilibrates at a higher density than surface waters. These deep export pathways may play a more complex role changing stratification in the subpolar North Atlantic as the ice sheet continues to lose mass. The connection between Greenland freshwater flux and stratification of the North Atlantic is an important, and poorly understood, way that changes in the ice sheet might drive changes in the buoyancy-driven large-scale ocean circulation [Lazier, 1980; Fichefet, 2003].

The composition of GMW indicates that the primary source of heat to the termini of Kangil and Eqip is PW and WPW, not AW, at least in late summer. AW is blocked by a narrow shallow sill close to the glacier, a type of bathymetric feature that easily goes unobserved in Greenland's fjords where reliable bathymetry is scarce [Rignot et al., 2015]. The noble gas OMP decomposition of GMW prevents the mistake of assuming that the AW heat is available for melting the glacier. This result shows that significant reservoirs of heat observed in a fjord sometimes are not available to melt ice at the glacier.

Quantifying the composition of GMW illustrates the major impact glacial buoyancy forcing has on upwelling water masses. We see that approximately PW volumes 30 times larger than the combined SMR and SMW volume flux are upwelled in Atå Sund.

The OMP decomposition reveals aspects of the ice-ocean boundary processes. The SMW/SMR ratio of the near-surface GMW implies that SMW is at least 26% of SMR volume flux. This suggests higher relative melt rates compared with previous work [Rignot *et al.*, 2010].

The radiogenic Helium signal suggests that substantial basal melting occurs in the englacial hydrological system, though some ambiguity in the AIM origin warrants further investigation of this finding.

We see indications of heterogeneous melt processes at the ice edge, where SMR-driven melt plumes produce a near-surface GMW layer, and more diffuse thermal melting creates a deep layer of GMW mostly composed of SMW. These results indicate that numerical models of ice-ocean interactions need to include both melt regimes.

#### Acknowledgments

Data used in this work are available by e-mailing the corresponding author. We gratefully acknowledge funding from WHOI's Ocean and Climate Change Institute, the Doherty Postdoctoral Scholarship, and ship time from the Advanced Climate Dynamics Summer School (SIU grant NNA-2012/10151). We thank K. Cahill for sample extraction and D.E. Lott III for assistance with noble gas and helium isotope measurements. We also thank R.H. Jackson, A. Vieli, K. Nisancioglu, and B. Loose for help with data collection and/or helpful discussion.

The Editor thanks two anonymous reviewers for their assistance in evaluating this paper.

#### References

- Bamber, J., M. R. van den Broeke, J. Ettema, J. Lenaerts, and E. Rignot (2012), Recent large increases in freshwater fluxes from Greenland into the North Atlantic, *Geophys. Res. Lett.*, *39*, L19501, doi:10.1029/2012GL052552.
- Bartholomaeus, T. C., C. F. Larsen, and S. O'Neel (2013), Does calving matter? Evidence for significant submarine melt, *Earth Planet. Sci. Lett.*, *380*(C), 21–30, doi:10.1016/j.epsl.2013.08.014.
- Bendtsen, J., J. Mortensen, K. Lennert, and S. Rysgaard (2015), Heat sources for glacial ice melt in a west Greenland tidewater outlet glacier fjord: The role of subglacial freshwater discharge, *Geophys. Res. Lett.*, *42*, 4089–4095, doi:10.1002/2015GL063846.
- Chauché, N., A. Hubbard, J. C. Gascard, J. E. Box, R. Bates, M. Koppes, A. Sole, P. Christoffersen, and H. Patton (2014), Ice-ocean interaction and calving front morphology at two west Greenland tidewater outlet glaciers, *Cryosphere*, *8*(4), 1457–1468, doi:10.5194/tc-8-1457-2014.
- Chu, V. W. (2014), Greenland ice sheet hydrology: A review, *J. Phys. Oceanogr.*, *38*(1), 19–54, doi:10.1177/0309133313507075.
- Craig, H., and P. Scarsi (1997), Helium isotope stratigraphy in the GISP-2 ice core, *EOS Trans. AGU*, *78*, 7.
- Craig, H., Y. Horibe, and T. Sowers (1988), Gravitational separation of gases and isotopes in polar ice caps, *Science*, *242*(4886), 1675–1678.
- Fichefet, T. (2003), Implications of changes in freshwater flux from the Greenland ice sheet for the climate of the 21st century, *Geophys. Res. Lett.*, *30*(17), 1911, doi:10.1029/2003GL017826.
- Foldvik, A., T. Gammelsrød, S. Østerhus, E. Fahrbaach, G. Rohardt, M. Schröder, K. Nicholls, L. Padman, and R. Woodgate (2004), Ice shelf water overflow and bottom water formation in the southern Weddell Sea, *J. Geophys. Res.*, *109*, C02015, doi:10.1029/2003JC002008.
- Gade, H. G. (1979), Melting of ice in sea water: A primitive model with application to the Antarctic ice shelf and icebergs, *J. Phys. Oceanogr.*, *9*, 189–198.
- Gladish, C., D. Holland, and C. Lee (2015), Oceanic boundary conditions for Jakobshavn Glacier: Part II. Provenance and sources of variability of Disko Bay and Ilulissat Icefjord waters, 1990–2011, *J. Phys. Oceanogr.*, *45*(1), 33–63, doi:10.1175/JPO-D-14-0045.1.
- Hamme, R., and J. Severinghaus (2007), Trace gas disequilibria during deep-water formation, *Deep Sea Res., Part I*, *54*, 939–950.
- Hanna, E., et al. (2013), Ice-sheet mass balance and climate change, *Nature*, *498*(7452), 51–59, doi:10.1038/nature12238.
- Hohmann, R., P. Schlosser, S. Jacobs, A. Ludin, and R. Weppernig (2002), Excess helium and neon in the southeast Pacific: Tracers for glacial meltwater, *J. Geophys. Res.*, *107*(C11), 3198, doi:10.1029/2000JC000378.
- Holland, D. M., R. H. Thomas, B. de Young, M. H. Ribergaard, and B. Lyberth (2008), Acceleration of Jakobshavn Isbræ triggered by warm subsurface ocean waters, *Nat. Geosci.*, *1*(10), 659–664, doi:10.1038/ngeo316.
- Hood, E., B. Howes, and W. Jenkins (1998), Dissolved gas dynamics in a perennially ice-covered Lake Fyell, Antarctica, *Limnol. Oceanogr.*, *43*, 265–272.
- Inall, M. E., T. Murray, F. R. Cottier, K. Scharrer, T. J. Boyd, K. J. Heywood, and S. L. Bevan (2014), Oceanic heat delivery via Kangerdlugssuaq Fjord to the south-east Greenland ice sheet, *J. Geophys. Res. Oceans*, *119*, 631–645, doi:10.1002/2013JC009295.
- Jackson, R. H., F. Straneo, and D. A. Sutherland (2014), Externally forced fluctuations in ocean temperature at Greenland glaciers in non-summer months, *Nat. Geosci.*, *7*(7), 503–508, doi:10.1038/ngeo2186.
- Jenkins, A. (1999), The impact of melting ice on ocean waters, *J. Phys. Oceanogr.*, *29*(9), 2370–2381.
- Jenkins, A. (2011), Convection-driven melting near the grounding lines of ice shelves and tidewater glaciers, *J. Phys. Oceanogr.*, *41*(12), 2279–2294, doi:10.1175/JPO-D-11-03.1.
- Jenkins, W., D. Lott, B. Longworth, J. Curtice, and K. Cahill (2014), The distributions of helium isotopes and tritium along the U.S. GEOTRACES North Atlantic sections (GEOTRACES GAO3), *Deep Sea Res., Part II*, *116*, 21–28, doi:10.1016/j.dsr2.2014.11.017.
- Kimura, S., P. R. Holland, A. Jenkins, and M. Piggott (2014), The effect of meltwater plumes on the melting of a vertical glacier face, *J. Phys. Oceanogr.*, *44*(12), 3099–3117, doi:10.1175/JPO-D-13-0219.1.
- Lazier, J. R. (1980), Oceanographic conditions at Ocean Weather Ship Bravo, 1964–1974, *Atmos. Ocean*, *18*(3), 227–238, doi:10.1080/07055900.1980.9649089.
- Loose, B., and W. J. Jenkins (2014), The five stable noble gases are sensitive unambiguous tracers of glacial meltwater, *Geophys. Res. Lett.*, *41*, 2835–2841, doi:10.1002/2013GL058804.
- Loose, B., P. Schlosser, W. M. Smethie, and S. Jacobs (2009), An optimized estimate of glacial melt from the Ross Ice Shelf using noble gases, stable isotopes, and CFC transient tracers, *J. Geophys. Res.*, *114*, C08007, doi:10.1029/2008JC005048.
- Martinerie, P., D. Raynaud, D. Etheridge, J. Barnola, and D. Mazaudier (1992), Physical and climatic parameters which influence the air content in polar ice, *Earth Planet. Sci. Lett.*, *112*, 1–13.
- Mortensen, J., J. Bendtsen, R. J. Motyka, K. Lennert, M. Truffer, M. Fahnestock, and S. Rysgaard (2013), On the seasonal freshwater stratification in the proximity of fast-flowing tidewater outlet glaciers in a sub-Arctic sill fjord, *J. Geophys. Res. Oceans*, *118*, 1382–1395, doi:10.1002/jgrc.20134.
- Nick, F. M., A. Vieli, M. L. Andersen, I. Joughin, A. Payne, T. L. Edwards, F. Pattyn, and R. S. W. van de Wal (2014), Future sea-level rise from Greenland's main outlet glaciers in a warming climate, *Nature*, *497*(7448), 235–238, doi:10.1038/nature12068.
- Rignot, E., M. Koppes, and I. Velicogna (2010), Rapid submarine melting of the calving faces of west Greenland glaciers, *Nat. Geosci.*, *3*(3), 187–191, doi:10.1038/ngeo765.



- Rignot, E., I. Fenty, Y. Xu, C. Cai, and C. Kemp (2015), Undercutting of marine-terminating glaciers in west Greenland, *Geophys. Res. Lett.*, *42*, 5909–5917, doi:10.1002/2015GL064236.
- Schlosser, P. (1986), Helium: A new tracer in Antarctic oceanography, *Nature*, *321*, 233–235.
- Sciascia, R., F. Straneo, C. Cenedese, and P. Heimbach (2013), Seasonal variability of submarine melt rate and circulation in an east Greenland fjord, *J. Geophys. Res. Oceans*, *118*, 2492–2506, doi:10.1002/jgrc.20142.
- Slater, D. A., P. W. Nienow, T. R. Cowton, D. N. Goldberg, and A. J. Sole (2015), Effect of near-terminus subglacial hydrology on tidewater glacier submarine melt rates, *Geophys. Res. Lett.*, *42*, 2861–2868, doi:10.1002/2014GL062494.
- Stanley, R., W. Jenkins, D. Lott, and S. Doney (2009), Noble gas constraints on air-sea gas exchange and bubble fluxes, *J. Geophys. Res.*, *114*, C11020, doi:10.1029/2009JC005396.
- Straneo, F., and P. Heimbach (2013), North Atlantic warming and the retreat of Greenland's outlet glaciers, *Nature*, *504*(7478), 36–43, doi:10.1038/nature12854.
- Straneo, F., R. G. Curry, D. A. Sutherland, G. S. Hamilton, C. Cenedese, K. Våge, and L. A. Stearns (2011), Impact of fjord dynamics and glacial runoff on the circulation near Helheim Glacier, *Nat. Geosci.*, *4*(5), 322–327, doi:10.1038/ngeo1109.
- Straneo, F., D. A. Sutherland, and D. Holland (2012), Characteristics of ocean waters reaching Greenland's glaciers, *Ann. Glaciol.*, *53*, 202–210, doi:10.3189/2012AoG60A059.
- Straneo, F., et al. (2013), Challenges to understanding the dynamic response of Greenland's marine terminating glaciers to oceanic and atmospheric forcing, *Bull. Am. Meteorol. Soc.*, *94*(8), 1131–1144, doi:10.1175/BAMS-D-12-00100.1.
- Sutherland, D. A., and F. Straneo (2012), Estimating ocean heat transports and submarine melt rates in Sermilik Fjord, Greenland, using lowered acoustic Doppler current profiler (LADCP) velocity profiles, *Ann. Glaciol.*, *53*(60), 50–58, doi:10.3189/2012AoG60A050.
- Tomczak, M., and D. G. B. Large (1989), Optimum multiparameter analysis of mixing in the thermocline of the eastern Indian Ocean, *J. Geophys. Res.*, *94*(C11), 16,141–16,149, doi:10.1029/JC094iC11p16141.
- Wells, A., and M. Worster (2008), A geophysical-scale model of vertical natural convection boundary layers, *J. Fluid Mech.*, *609*, 111–137, doi:10.1017/S0022112008002346.
- Xu, Y., E. Rignot, I. Fenty, D. Menemenlis, and M. M. Flexas (2013), Subaqueous melting of Store Glacier, west Greenland from three-dimensional, high-resolution numerical modeling and ocean observations, *Geophys. Res. Lett.*, *40*, 4648–4653, doi:10.1002/grl.50825.